

PORE-SCALE SIMULATION OF HIGH-DENSITY-RATIO MULTIPHASE FLOWS IN POROUS MEDIA USING LATTICE BOLTZMANN METHOD

Haihu Liu*, Albert J. Valocchi* and Qinjun Kang[†]

*University of Illinois at Urbana-Champaign
Department of Civil and Environmental Engineering, Urbana, IL 61801 USA

[†] Los Alamos National Laboratory
Earth and Environmental Sciences Division, Los Alamos, NM 87545 USA

Key words: porous media, multiphase flows, high-density-ratio, lattice Boltzmann method

Summary. A lattice Boltzmann high-density-ratio model, which uses diffuse interface theory to describe the interfacial dynamics and was proposed originally by Lee and Liu [T. Lee, L. Liu, Lattice Boltzmann simulations of micron-scale drop impact on dry surfaces, *J. Comput. Phys.* 229(2010) 8045-8063], is extended to simulate multiphase flows in porous media. A wetting boundary treatment is proposed for the concave and convex corners. Capability and accuracy of this model is validated by simulations of equilibrium contact angle, and the injection of a non-wetting gas into two parallel capillaries. This model is also used to simulate immiscible displacement in a micromodel, and some interesting phenomena are observed.

1 INTRODUCTION

Understanding multiphase displacement in porous media, especially from a pore-scale viewpoint, is important in a variety of fields, such as groundwater hydrology and petroleum engineering. However, such an understanding is complicated due to a large number of factors influencing the flows, such as fluid density and viscosity, surface tension, wetting properties and heterogeneity of the porous media, fluid flow rates, and the considered length scales. Although experimental studies have helped to understand multiphase flows in porous systems, it is still challenging to accurately visualize the position of phase interfaces especially in 3D pore geometries, and to measure the detailed pressure distribution and velocity field due to the dynamic behavior and the limitation of experimental technique. Numerical simulations can be complementary to the experimental studies, and provide an economic and efficient pathway to explore the influence of flow and physical parameters in porous media. Recently developed lattice Boltzmann method (LBM)

is particularly suitable for simulating pore-scale flows in porous media. It is capable of handling arbitrarily complex geometries¹, and its mesoscopic nature can provide many advantages of molecular dynamics, making the LBM especially useful for simulation of multiphase flows^{2,3}. Numerical simulation of multiphase flows with high density ratio (HDR) is a daunting task. There has been an ongoing effort to improve the stability of LBM for HDR multiphase flows⁴⁻⁶. However, until today, no study has reported using LBM to simulate HDR multiphase flows in porous media. Here we develop a LBM approach for pore-scale simulations of HDR multiphase flows in porous media, in which a wetting boundary treatment is proposed for concave and convex corners. Several numerical simulations are conducted to validate the feasibility and accuracy of this approach.

2 NUMERICAL METHOD

2.1 Governing equation and diffuse interface theory

We consider here a lattice Boltzmann diffuse interface model⁶ for incompressible immiscible two-phase flows with different densities and viscosities. Suppose that there are two incompressible immiscible fluids, say gas and liquid. The order parameter C is defined as the volume fraction of one of the two phases. Thus, C is assumed to be constant in the bulk phases, e.g. $C = 0$ for the gas phase while $C = 1$ for the liquid phase. Across the interfacial region, there is a rapid but smooth change of C . The time evolution of the diffuse interface is governed by the following Cahn-Hilliard equation (CHE)⁶,

$$\partial_t C + \vec{u} \cdot \nabla C = M \nabla^2 \mu \quad (1)$$

where \vec{u} is the flow velocity, and M is the mobility. The chemical potential μ in Eq.(1) can be derived from the free-energy functional

$$\Psi = \int_V \psi(C, \nabla C) dV = \int_V \left[\beta C^2 (1 - C)^2 + \frac{\kappa}{2} |\nabla C|^2 \right] dV \quad (2)$$

where β is a constant, and κ is a coefficient related to the surface tension. By minimizing the free energy functional, the chemical potential is given by

$$\mu = \frac{\delta \Psi}{\delta C} = 2\beta C(C - 1)(2C - 1) - \kappa \nabla^2 C \quad (3)$$

For a planar gas-liquid interface in a quiescent infinite system, the order parameter profile across the interface can be obtained from Eq.(3) at $\mu = 0$,

$$C(z) = \frac{1}{2} + \frac{1}{2} \tanh \left(\frac{z}{\xi} \right) \quad (4)$$

where z is the spatial location normal to the interface ($z = 0$), and ξ is a measure for the thickness of interface, which is defined as $\xi = \sqrt{\frac{2\kappa}{\beta}}$.

The surface tension σ can be interpreted as the excess free energy per unit interface area, and for a planar interface in equilibrium, it can be evaluated by

$$\sigma = \int_{-\infty}^{\infty} \kappa |\nabla C|^2 dz = \frac{\kappa}{3\xi} \quad (5)$$

With consideration of surface tension, the governing equations for the incompressible fluid flows can be written as⁶:

$$\nabla \cdot \vec{u} = 0, \quad (6)$$

$$\rho(\partial_t \vec{u} + \vec{u} \cdot \nabla \vec{u}) = -\nabla p - C \nabla \mu + \nabla \cdot [\eta(\nabla \vec{u} + \nabla \vec{u}^T)], \quad (7)$$

where p is pressure, and $\rho = C\rho_L + (1 - C)\rho_G$ is the average density; similarly, $\eta = C\eta_L + (1 - C)\eta_G$ is the average viscosity. In this study, we use the subscripts ‘L’ and ‘G’ denote liquid phase and gas phase, respectively.

To ensure mass conservation, there should be no diffuse flux penetrating the wall, i.e.,

$$\vec{n} \cdot \nabla \mu|_w = 0, \quad (8)$$

where \vec{n} is the unit vector normal to the wall. For flows with contact-line dynamics, the wetting condition proposed by Lee and Liu⁶ is imposed at the solid wall, which provides the boundary condition for the order parameter C ,

$$\vec{n} \cdot \nabla C|_w = \sqrt{2\beta/\kappa} \Omega_c (C - C^2) \quad (9)$$

where Ω_c is the dimensionless wetting potential, which is related to the equilibrium contact angle θ^{eq} by Young’s law⁶:

$$\cos(\theta^{eq}) = \frac{\sigma_{SG} - \sigma_{SL}}{\sigma} = -\Omega_c \quad (10)$$

where $\sigma_{SG}(\sigma_{SL})$ is the surface tension between gas(liquid) and the solid surface.

2.2 Lattice Boltzmann method

The Navier-Stokes equations(NSEs) and CHE are solved in a LBM framework following Lee and Liu⁶. The evolution equations of particle distribution functions(PDFs) are derived through the discrete Boltzmann equation(DBE) with the trapezoidal rule applied along characteristics. To ensure the numerical stability in solving HDR problems, the second-order mixed difference is applied to discretize the derivatives involved in forcing terms in the pre-streaming collision step while the standard central difference in the post-streaming collision step. The evolution equations of PDFs are,

$$\begin{aligned} g_\alpha(\vec{x} + \vec{e}_\alpha \delta_t, t + \delta_t) - g_\alpha(\vec{x}, t) &= \frac{1}{\tau+1/2} [g_\alpha^{eq}(\vec{x}, t) - g_\alpha(\vec{x}, t)] \\ &+ \delta_t (\vec{e}_\alpha - \vec{u}) \cdot [\nabla^M \rho c_s^2 (\Gamma_\alpha - w_\alpha) - C \nabla^M \mu \Gamma_\alpha]_{(\vec{x}, t)} \end{aligned} \quad (11)$$

$$\begin{aligned} h_\alpha(\vec{x} + \vec{e}_\alpha \delta_t, t + \delta_t) &= h_\alpha^{eq}(\vec{x}, t) + \frac{\delta_t}{2} M \nabla^2 \mu \Gamma_\alpha|_{(\vec{x}, t)} \\ &+ \frac{\delta_t}{2} M \nabla^2 \mu \Gamma_\alpha|_{(\vec{x} + \vec{e}_\alpha \delta_t, t)} + \delta_t (\vec{e}_\alpha - \vec{u}) \cdot \left[\nabla^M C - \frac{C}{\rho c_s^2} (\nabla^M p + C \nabla^M \mu) \right] \Gamma_\alpha|_{(\vec{x}, t)} \end{aligned} \quad (12)$$

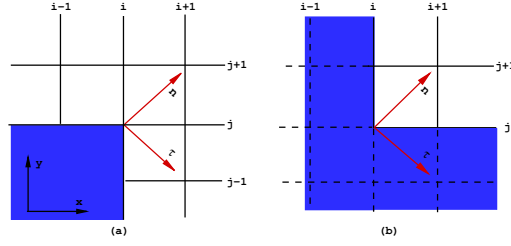


Figure 1: Transition nodes at the intersections of two orthogonal walls: (a)convex and (b)concave.

with

$$\Gamma_\alpha = \Gamma_\alpha(\vec{u}) = w_\alpha \left[1 + \vec{e}_\alpha \cdot \vec{u} / (c_s^2) + (\vec{e}_\alpha \cdot \vec{u})^2 / (2c_s^4) - \vec{u} \cdot \vec{u} / (2c_s^2) \right] \quad (13)$$

where g_α and h_α are the PDFs for the momentum and the order parameter, respectively, and g_α^{eq} and h_α^{eq} are the corresponding equilibrium PDFs. τ is the dimensionless relaxation time, \vec{e}_α is the lattice velocity, w_α is the weight factor, and c_s is the speed of sound. The subscript ‘ M ’ on gradient means that the second-order mixed difference is used to discretize the derivative, while the subscript ‘ C ’, as shown below, means that the second-order central difference is used⁶.

For a two-dimensional 9-velocity model (D2Q9)¹, the lattice velocities are $\vec{e}_0 = (0, 0)$, $\vec{e}_{1,3} = (\pm c, 0)$, $\vec{e}_{2,4} = (0, \pm c)$, $\vec{e}_{5,7} = (\pm c, \pm c)$ and $\vec{e}_{6,8} = (\mp c, \pm c)$. The lattice speed c is defined by $c = \delta_x / \delta_t$, where δ_x and δ_t are the lattice distance and the time step, respectively. The sound speed is related to c by $c_s = c / \sqrt{3}$. The equilibrium PDFs are,

$$g_\alpha^{eq} = w_\alpha (p - \rho c_s^2) + \rho c_s^2 \Gamma_\alpha - \frac{\delta_t}{2} (\vec{e}_\alpha - \vec{u}) \cdot [\nabla^C \rho c_s^2 (\Gamma_\alpha - w_\alpha) - C \nabla^C \mu \Gamma_\alpha] \quad (14)$$

$$h_\alpha^{eq} = C \Gamma_\alpha - \frac{\delta_t}{2} (\vec{e}_\alpha - \vec{u}) \cdot \left[\nabla^C C - \frac{C}{\rho c_s^2} (\nabla^C p + C \nabla^C \mu) \right] \Gamma_\alpha \quad (15)$$

where $w_0 = 4/9$, $w_{1-4} = 1/9$ and $w_{5-8} = 1/36$.

Using the Chapman-Enskog expansion, Eqs.(11) and (12) approximately recover the NSEs and the CHE with the second order accuracy. The dynamic viscosity in the NSEs derived from Eq.(11) is $\eta = \rho \tau c_s^2 \delta_t$. The macroscopic fluid variables are calculated by

$$C = \sum_\alpha h_\alpha, \quad \rho \vec{u} = \frac{1}{c_s^2} \sum_\alpha g_\alpha \vec{e}_\alpha - \frac{\delta_t}{2} C \nabla^C \mu, \quad p = \sum_\alpha g_\alpha + \frac{\delta_t}{2} \vec{u} \cdot \nabla^C \rho c_s^2 \quad (16)$$

2.3 Boundary conditions

No-slip boundary condition is applied at solid walls using the bounce-back scheme⁶. To obtain a specified contact angle, Eqs.(8) and (9) are implicitly imposed through $\nabla^2 \mu$ and $\nabla^2 C$ at the solid walls, respectively. For a straight wall, for example, the bottom wall, the Laplacian operator of ϕ (μ or C) at position (i, j) can be easily evaluated by

$$\nabla^2 \phi|_{i,j} = \frac{\phi_{i+1,j} - 2\phi_{i,j} + \phi_{i-1,j}}{\delta_x^2} + 2 \frac{\phi_{i,j+1} - \phi_{i,j} - \frac{\partial \phi}{\partial n}|_w \delta_x}{\delta_x^2} \quad (17)$$

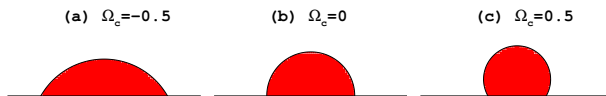


Figure 2: Liquid droplet on a solid surface with the wetting potential Ω_c of -0.3 (a), 0 (b) and 0.3 (c).

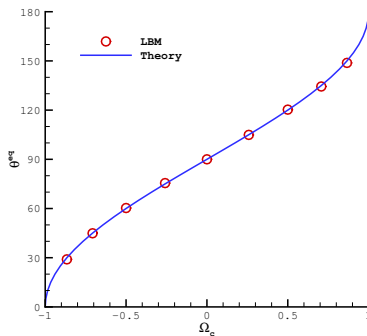


Figure 3: The simulated equilibrium contact angles vs. the theoretical predictions by Eq.(10).

which has been introduced by Lee and Liu⁶. In this study, we extend this model to treat non-smooth solid surfaces. Here only boundary nodes at the intersection of two perpendicular lines, encountered in our 2D pore-scale simulations, are discussed. In order to relieve the singularity of the derivative at these corner nodes, it is imagined that there virtually exist inclined planes as a transition between the horizontal and vertical planes. On the transitional nodes, the Laplacian operator can be evaluated directly by the normal and tangential derivatives in the inclined coordinate system. For the convex corner node in Fig. 1(a), the Laplacian $\nabla^2\phi$ is evaluated as

$$\nabla^2\phi|_{i,j} = \frac{\phi_{i+1,j-1} - 2\phi_{i,j} + \phi_{i-1,j+1}}{2\delta_x^2} + \frac{\phi_{i+1,j+1} - \phi_{i,j} - \sqrt{2}\frac{\partial\phi}{\partial n}|_w\delta_x}{\delta_x^2} \quad (18)$$

For the concave corner node (see Fig. 1(b)), the neighboring nodes at $(i-1, j+1)$ and $(i+1, j-1)$ are out of the domain, some additional approximations need to be used, specifically, they are $\phi_{i-1,j+1} \approx \phi_{i,j+1}$ and $\phi_{i+1,j-1} \approx \phi_{i+1,j}$. In addition, the buried PDFs ($g_{6,8}$ and $h_{6,8}$) are unknown for the concave nodes after the streaming step, so the value of the order parameter is unknown. To proceed with the subsequent collision step, we approximate the buried PDFs by averaging the sum of pre-streaming, buried PDFs.

3 NUMERICAL SIMULATIONS

3.1 Equilibrium droplet on solid surfaces

The static contact angle simulations are performed in a 200×100 lattice domain. The initial condition is a semicircular stationary liquid droplet with radius $R = 25$ sitting along the center line on the bottom wall. The top wall is assumed to be neutral wetting,

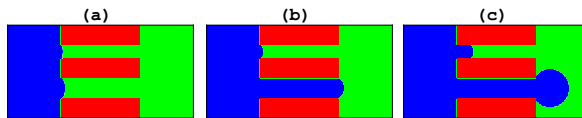


Figure 4: Injection of a non-wetting gas into two parallel capillary tubes with pressure difference Δp of 4×10^{-5} (a), 6×10^{-5} (b), and 8×10^{-5} (c).

i.e. $\theta^{eq} = 90^\circ$. The periodic boundary condition is used in the x -direction while the bounce-back boundary condition is imposed at top and bottom in the y -direction. The densities of both fluids are fixed at $\rho_L = 1.0$ and $\rho_G = 1.188 \times 10^{-3}$, in which case the surface tension is $\sigma = 1 \times 10^{-4}$. Other parameters are chosen as: $\xi = 2.5$, $\tau = 0.2$, and $M = 0.02/\beta$. We run the simulation until the droplet shape does not change, i.e. reaching an equilibrium state. Different contact angles can be achieved through adjusting the dimensionless wetting potential Ω_c according to Eq.(9). Fig. 2(a)-(c) shows equilibrium shapes of the droplet with the wetting potential $\Omega_c = -0.5, 0$ and 0.5 , respectively. Their corresponding equilibrium contact angles, calculated from the measured droplet height and base diameter, are $60.3^\circ, 90^\circ$ and 120.3° , respectively. The simulated equilibrium contact angle as a function of the wetting potential for a wider range is presented in Fig. 3, where it is shown that the simulated results by the present LBM agree quite well with the theoretical solution, Eq.(10), in the range of contact angle from 30° to 150° .

3.2 Injection of non-wetting gas into two parallel capillaries

We consider the injection of a non-wetting gas through two parallel capillary tubes, a case that is used to assess whether the HDR model is able to capture capillary effect and reproduce correct displacement behavior. As shown in Fig. 4, the widths of the upper and lower capillary tubes are r_1 and r_2 ($r_1 < r_2$), and P_{c1} and P_{c2} are the corresponding capillary threshold pressures. These capillary threshold pressures can be determined analytically by a combination of surface tension, contact angle and widths of tube⁷,

$$P_{c1} = 2\sigma \cos(\theta)/r_1, \quad P_{c2} = 2\sigma \cos(\theta)/r_2 \quad (19)$$

We specify a uniform pressure p_{in} at the left inlet and p_{out} at the right outlet. Initially, the invading gas is just located at the entrances of the two capillary tubes. The displacement behavior is determined by the pressure difference $\Delta p = p_{in} - p_{out}$ and the capillary threshold pressures. Simulations are run in a 280×140 lattice domain with the widths of two capillary tubes $r_1 = 20$ lattices and $r_2 = 30$ lattices, respectively. The simulation parameters are chosen as $\rho_L = 1.0$, $\rho_G = 0.01$, $\sigma = 1 \times 10^{-3}$, $\tau = 0.3$, $\xi = 4$ and $\theta = 45^\circ$. With these parameters, the capillary threshold pressures can be calculated by Eq.(19) and they are $P_{c1} = 7.1 \times 10^{-5}$ and $P_{c2} = 4.7 \times 10^{-5}$. Three different pressure differences are simulated in this study: $\Delta p = 4 \times 10^{-5}$, 6×10^{-5} , and 8×10^{-5} , and the corresponding simulation results are shown in Fig. 4. Obviously, when Δp is smaller than P_{c2} (Fig. 4(a)), the invading gas cannot enter both capillary tubes. When Δp is

between P_{c2} and P_{c1} (Fig. 4(b)), the gas only flows into the large tube. When the pressure difference is increased to $\Delta p > P_{c1}$ (Fig. 4(b)), the gas flows into both capillary tubes, but displacement is much faster in the large tube. This displacement behavior is in agreement with the theoretical analysis, which is the principle of pore-network simulators⁷.

3.3 Immiscible displacement in a micromodel

The HDR model is used to simulate immiscible fluid displacement in a 2D horizontal micromodel. The pore network in the micromodel consists of staggered arrays of identical square grains with sides of $l = 40$ lattices. The grains are arranged in a periodic pattern with unit cell of around 100 lattices in length. In order to produce the fingers, small perturbations are introduced in the simulations. Specifically, the location of each grain center is generated by the perfectly arranged coordinate plus a random perturbation between -1 and 1 in both x and y directions. The non-wetting gas is injected at a constant flow rate at the left inlet, while a constant pressure is imposed at the right outlet. The lateral boundaries are assumed to be solid walls. The simulation is carried out in a 1728×1200 lattice domain with the density and viscosity ratios of liquid-to-gas being 100. The contact angle is chosen to be $\theta = 45^\circ$, and the capillary number is $Ca = 10^{-4}$, where $Ca = \frac{u_{in}\eta_G}{\sigma \cos \theta}$, and u_{in} is the mean velocity of the advancing gas at inlet.

We run the simulation until the injected gas reaches the outlet boundary, when ‘break-through’ is thought to have occurred. Fig. 5 shows the evolution of non-wetting phase distribution in micromodel at times $t^* = \{2.5, 5, 7.5, 9.6\}$, where $t^* = u_{in}t/l$ is the dimensionless time. Fingering is clearly observed during the displacement, in which several independent interconnected flow paths progress forward toward the outlet. In our simulation, the formation of fingers is attributed to the small perturbation in position of grains, whereas in an experiment, it may be attributed to non-uniformity in grain size, grain position, or in the depth of flow channel (3D effects), due to microfabrication technology. We can also observe that the pore body is almost occupied completely by the invading gas before the gas can reach a neighboring pore. This observation is consistent with the assumption introduced by Lenormand et al.⁷ in pore-network simulations. In addition, the non-wetting gas progresses from a pore through the largest pore throat in any direction, and therefore may progress into new pore in the backward direction (see the circle inside in Fig. 5(d)), which are the typical characteristics of capillary fingering. When the liquid is trapped, the interface between gas and liquid keeps an angle of around 45° with the grain surface, close to the prescribed equilibrium contact angle. This indicates that the trapped fluid approaches the equilibrium state.

4 CONCLUSIONS

A lattice Boltzmann high-density-ratio model, proposed originally by Lee and Liu⁶, is extended for pore-scale simulations of multiphase flows in porous media. We propose a wetting boundary treatment for concave and convex corners, which can be extended to

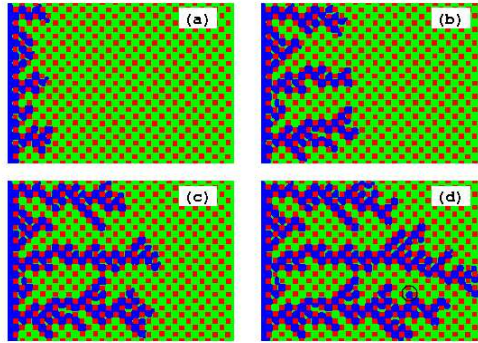


Figure 5: Non-wetting phase distribution(blue) in micromodel at times $t^* = \{2.5, 5, 7.5, 9.6\}$ for $Ca = 10^{-4}$, and $\rho_L/\rho_G = \eta_L/\eta_G = 100$.

more complicated geometries with curved boundaries. The usefulness and accuracy of this model is first validated by simulations of equilibrium contact angle, and the injection of a non-wetting gas into two parallel capillaries. This model is then used to simulate immiscible displacement in a micromodel, and some interesting phenomena are observed.

ACKNOWLEDGMENTS This paper is based upon work supported by the LDRD Program (#20100025DR) of the Los Alamos National Laboratory.

References

- [1] S. Succi. *The Lattice Boltzmann Equation for Fluid Dynamics and Beyond*. Oxford: Oxford University Press, (2001).
- [2] S. Chen and G.D. Doolen. Lattice Boltzmann method for fluid flows. *Annu. Rev. Fluid Mech.*, **30**, 329–364, (1998).
- [3] J. Zhang. Lattice Boltzmann method for microfluidics: models and applications. *Microfluid. Nanofluid.*, **10**, 1–28, (2011).
- [4] T. Inamuro, T. Ogata, S. Tajima, and N. Konishi. A lattice Boltzmann method for incompressible two-phase flows with large density differences. *J. Comput. Phys.*, **198**, 628–644, (2004).
- [5] T. Lee and C.-L. Lin. A stable discretization of the lattice Boltzmann equation for simulation of incompressible two-phase flows at high density ratio. *J. Comput. Phys.*, **206**, 16–47, (2005).
- [6] T. Lee and L. Liu. Lattice Boltzmann simulations of micron-scale drop impact on dry surfaces. *J. Comput. Phys.*, **229**, 8045–8063, (2010).
- [7] R. Lenormand, E. Touboul, and C. Zarcone. Numerical models and experiments on immiscible displacements in porous media. *J. Fluid Mech.*, **189**, 165–187, (1988).